journal

J. Am. Ceram. Soc., 96 [6] 1801–1809 (2013)
DOI: 10.1111/jace.12241

Degradation Analysis of the SnO_2 and ZnO-Based Varistors Using Electrostatic Force Microscopy

M. A. Ramírez,[‡,†] R. Tararam,[§] A. Z. Simões,[‡] A. Ries,[¶] E. Longo,[§] and J. A. Varela[§]

[‡]Faculdade de Engenharia de Guaratinguetá, Universidade Estadual Paulista (UNESP), Av. Dr. Ariberto Pereira da Cunha 333, CEP 12516-410 Guaratinguetá, São Paulo, Brazil

[§]Instituto de Química, Universidade Estadual Paulista (UNESP), Rua Prof. Francisco Degni, 55, CEP 14801-970 Araraquara, São Paulo, Brazil

[¶]Laboratório de Dispositivos e Nanoestruturas, Universidade Federal de Pernambuco (UFPE), Rua Acadêmico Hélio Ramos s/n, CEP 50740-330 Recife, Pernambuco, Brazil

The degradation phenomena of ZnO and SnO_2-based varistors were investigated for two different degradation methods: DC voltage at increased temperature and degradation with 8/20 μs pulsed currents (lightning type). Electrostatic force microscopy (EFM) was used to analyze the surface charge accumulated at grain-boundary regions before and after degradation. Before the degradation process, 85% of the barriers are active in the SnO_2 system, while the ZnO system presents only 30% effective barriers. Both systems showed changes in the electrical behavior when degraded with pulses. In the case of the ZnO system, the behavior after pulse degradation was essentially ohmic due to the destruction of barriers (about 99% of the interfaces are conductive). After the degradation with 8/20 μs pulsed currents, the SnO_2 system still presents nonohmic behavior with a significant decrease in the quantity of effective barriers (from 85% to 5%). However, when the degradation is accomplished with continuous current, the SnO_2 system exhibits minimum variation, while the ZnO system degrades from 30% to 5%. This result indicates the existence of metastable defects of low concentration and/or low diffusion in the SnO_2 system. High energy is necessary to degrade the barriers due to defect annihilation in the SnO_2 system.

I. Introduction

Varistors are nonlinear electroceramic devices with a microstructure consisting of conducting grains surrounded by insulating grain boundaries being used as protective devices against surge voltages in energy distribution and transmission lines.[1,2] The two most widely studied varistor materials are ZnO (Matsuoka system)[3] and SnO_2 (Pianaro system)[4]; an adequate doping leads to excellent nonlinear coefficients and low leakage currents. The advantages of SnO_2-based varistors seem to be intimately related to their simple microstructure and relatively low additive concentration necessary to attain nonohmic electrical properties. These varistors present excellent mechanical properties minimizing thermomechanical failures such as puncturing and/or cracking.[5] Stability against over-voltages is a key parameter related to the performance of varistors. The degradation process usually leads to the reduction in the potential barrier height and causes change in defect concentration near grain boundaries.[6,7] Although the degradation of the barriers has been extensively studied,[8–16] the role of the grain boundaries is particularly interesting. The presence of inactive grain boundaries and other important parameters affecting the current-voltage characteristic have been experimentally studied.[17–20] The ratio of effective and noneffective barriers and its influence on the varistor properties has also been evaluated.[21] Electrostatic force microscopy (EFM) is used to map the gradient of the electric field between the tip and the sample. The field can be induced by applying a voltage to the tip and the trapped charges in different regions of the sample are often sufficiently large to generate contrast in an EFM image.[22–24] It was used in this study in a qualitative way to gain a better understanding of degradation processes of potential barriers. However, a study evaluating the potential barriers before and after degradation by DC bias voltage and 8/20 μs pulsed currents (lightning type) by means of EFM has not been published yet in the literature. Therefore, in this study EFM was employed to evaluate two degradation processes in ZnO- and SnO_2-based varistors.

II. Experimental Procedure

The studied systems correspond to the commercial ZnO-based varistor (modified Matsuoka system) with the composition 95.4% ZnO + 1.5% Sb_2O_3 + 1% NiO + 0.1% SiO_2 + 0.5% (Bi_2O_3, SnO_2, Co_2O_3, MnO) [ZnO], and to the SnO_2-based system (Pianaro system) with the composition 98.9% SnO_2 + 1% CoO + 0.05% Nb_2O_5 + 0.05% Cr_2O_3 [SCNCr], where all dopants were given as molar percentages. The ceramic pellets were prepared from analytical grade raw materials by solid-state reaction as described in previous works.[3,4,25–27] Powders were prepared by the conventional mixed oxide method. Oxides were milled for 24 h using zirconia balls in isopropyl alcohol medium. Then the homogenized mixtures were pressed into disks of 12 mm diameter and 1.1 mm thickness followed by isostatic pressing at 210 MPa. ZnO-based samples were sintered at 1180°C for 2 h,[25] whereas SCNCr samples were sintered at 1300°C for 1 h.[4] The degradation by DC bias voltage is accelerated at increased temperature (thermal steady-state conditions) under a constant voltage level. The stability/instability against DC accelerated stress was performed with an applied electric field E equivalent to a current density of 0.05 mA/cm^2 during 24 h at constant temperatures: 25°C, 50°C, 75°C, 90°C, 100°C, and 110°C. For the SnO_2-based system, two additional temperatures were considered: 150°C and 200°C. The level of degradation was monitored for 24 h by measuring the leakage current every 3 s (using a Keithley 237 unit; Cleveland, OH) during the fixed voltage stress level at these

L. M. Levinson—contributing editor

Manuscript No. 31755. Received July 15, 2012; approved January 24, 2013.
[†]Author to whom correspondence should be addressed. e-mail: margbrasil@yahoo.com

different temperatures. High-voltage measurements were performed by means of a current generator adapted from a Haefely instrument (Haefely Test AG, Basel, Switzerland) that delivers 8/20 μs current pulses. The high voltage circuit was based on three capacitors with a total capacitance of 2.25 μF and maximum voltage and energy of 200 kV and 45 kJ, respectively. The response of the devices was registered with a Tektronix (8 bits, 100 MHz) digital oscilloscope. Because of the rapid varistor response (in the order of nanoseconds), the measurements registered with the Keithley unit can be perfectly superimposed to those obtained by pulse application. The samples were encapsulated prior to realization of the high voltage measurements. Encapsulation of the ceramic disks is a critical point of the device preparation as the selected material might influence the electrical response. To avoid or minimize failures of the electrical insulation, a polymeric resin resistant to high temperatures must be used.

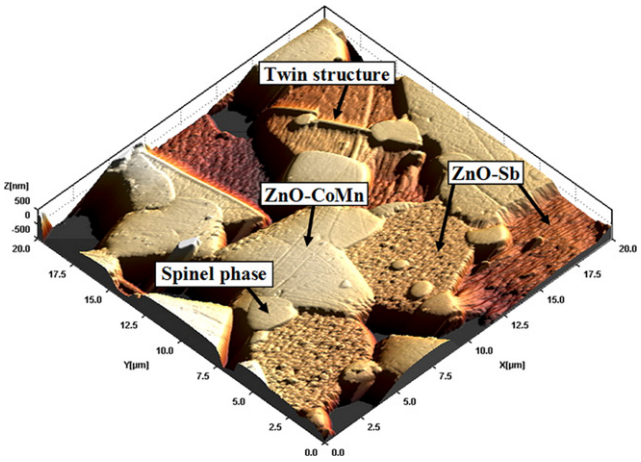

Fig. 1. AFM topographic 3-D image of the ZnO-based system prior to degradation and after chemical etching.

The impedance spectroscopy technique was used to calculate the potential barrier parameters, considering the variation in capacitance as a function of bias voltage applied to the varistor (C–V characteristic). Impedance spectroscopy was performed with a frequency response analyzer 4192 A LF HP (Santa Rosa, CA) using a frequency range from 5 Hz to 110 MHz and an oscillation amplitude of 0.5 V. A direct current potential (V_{cc}) was superimposed to the alternating potential, the range of V_{cc} used was 0–38 V.

Electrostatic force microscopy capabilities were implemented using commercial atomic force microscope (AFM Multimode NanoScope IIIA, Bruker, Billerica, MA). The topographic information was stored with a selectable height offset in EFM mode, during which the electric field data are collected simultaneously. The conductive tip (PtIr coating) was subjected to a range of voltages from 0 to 2 V to increase image contrast and the EFM scan was performed at a lift height of 50 nm. Percentages of electrically active barriers (%n_e) were calculated using the following relationship:

$$\%n_e = 100(n_e/n_t) \tag{1}$$

where n_e is the number of junctions with the accumulated charge (active barriers) and n_t is the total number of joints or boundaries.[28,29] The determination of the percentage of active barriers in each sample was a statistical process, and various regions of the sample were analyzed.

III. Results and Discussion

(1) Sample Properties Before Electrical Degradation

Figure 1 shows a topographic image of the microstructure using AFM of the multiphase polycrystalline ZnO-based system before electrical degradation. From the surface,

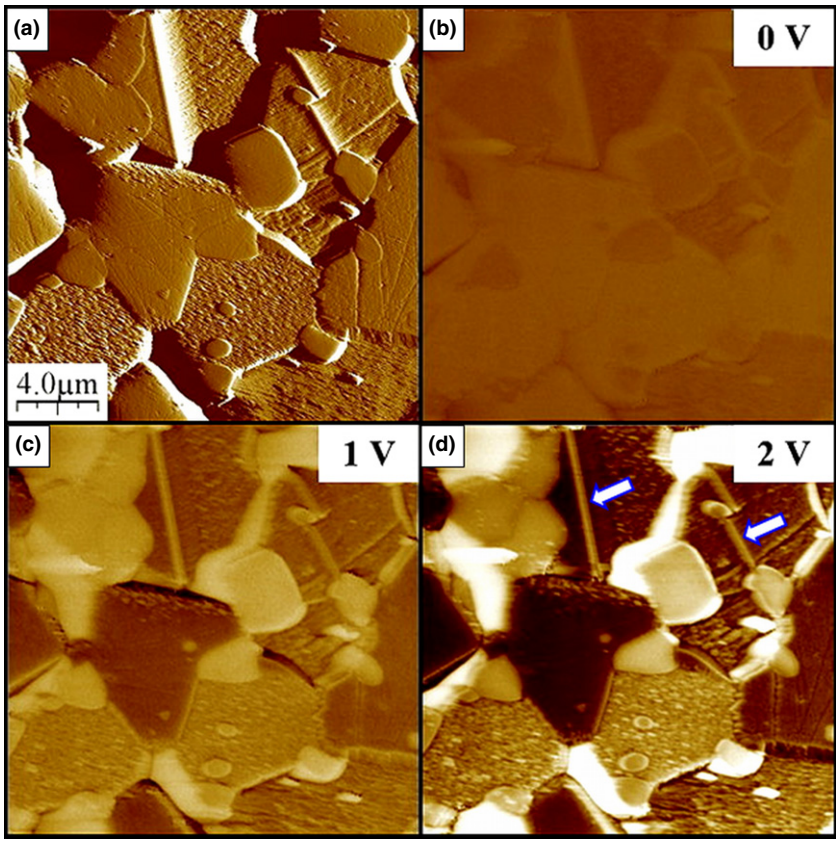

Fig. 2. (a) AFM topographic image of the ZnO-based system before electrical degradation. Series of EFM images without applied voltage (b), with applied voltage of 1 V (c), and 2 V (d). In Figure (d), arrows indicate active potential barriers.

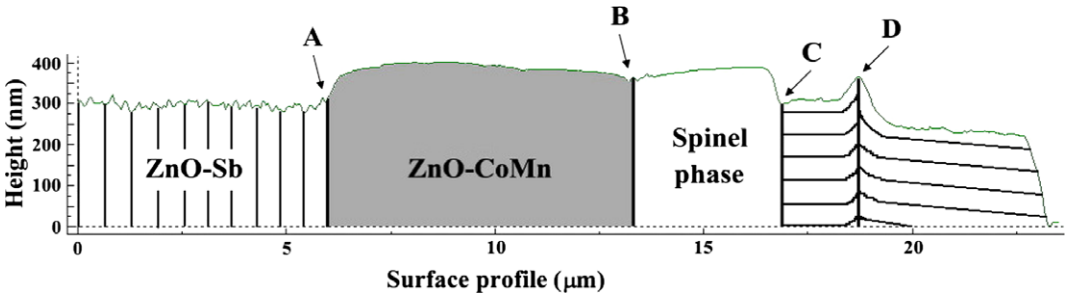

Fig. 3. AFM topography of ZnO varistor system showing the different phases and interfaces.

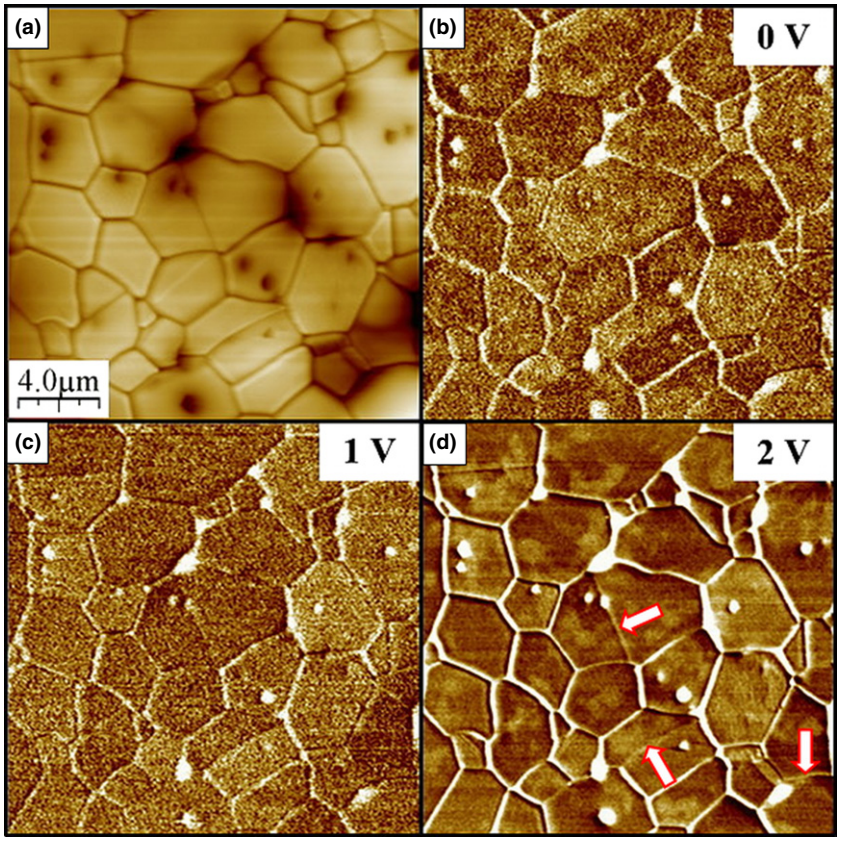

Fig. 4. (a) AFM topographic image of the SCNCr system before electrical degradation. Series of EFM images without applied voltage (b), with applied voltage of 1 V (c), and 2 V (d). In Figure (d), arrows indicate inactive potential barriers.

details of the corrosion intensity caused by a chemical attack on the different phases (two types of ZnO grains and a spinel phase) can be observed. The minor attacked regions correspond to grains of the spinel phase and ZnO–CoMn grains, while the most attacked regions correspond to antimony enriched grains, here named as ZnO–Sb (the difference of the two grain types of the zincite phase was found by energy dispersive spectroscopy and is not shown here). It is important to note that the ZnO–Sb grains form a twin structure, which is correlated with improved varistor behavior.[7,30]

Figure 2 corresponds to a topographical ZnO-based system and EFM images with voltage steps from 0 and 2 V applied to the tip. The bright grain regions are more resistive compared with dark grain and the electrical response of some grain boundaries are predominantly insulating. From Figs. 2 (b–d), a clear change in the electrical behavior depending on the bias applied becomes evident, indicating that the potential barrier formed in some of the grain boundaries are Schottky type [arrows showed in Fig. 2 (d)].[28,29] Effective barriers are difficult to find and these appear to be linked predominantly to the presence of twins. The percentage of effective barriers before degradation estimated from images with bias of 2 V using Eq. (1) was 30%. This result is in agreement with previous studies regarding this material (using other methodologies).[19,31–33]

In addition to the determination of effective barriers at the grain boundaries, the EFM technique also allows to study the different electrical responses in the grains of the main phase and secondary phases. This technique demonstrates the highly resistive behavior of the spinel phase; identified by bright grains in the image taken at 2 V. Due to its corrosion during chemical etching, the electrical response of the δ-Bi_2O_3 phase (also present in the ZnO-based varistors) was not evaluated.

To understand the microstructure of the material and its correlation with the nonohmic properties, Fig. 3 shows a schematic drawing of the different phases and identifies the interfaces in the ZnO-based varistors. The presence of different phases and interfaces explains the low number of effective barriers. The diagram shows the resistive region of the anisotropic ZnO–Sb phase, where interface **A** is reluctant to form an effective barrier due to the semiconductor character in that axis orientation. However, at interface **D** a

Table I. Parameters of the Potential Barrier Using the Model (*C–V*)[35] for the Different Varistor Systems Before Degradation Processes

Sample	ϕ_b (eV)	N_d (m^{-3})	N_{ES} (m^{-2})	ω (nm)
ZnO before degradation	1.03	6.86×0^{23}	2.50×10^{16}	18.2
SCNCr before degradation	1.65	1.50×10^{24}	6.19×10^{16}	20.6

plastic deformation of the ZnO–Sb phase generating a set of small substructures named twins, where there is high probability of effective barrier formation, as these substructures concentrate a reasonable level of mechanical stresses and defects where oxygen species are easily adsorbed.[34] It is well known that the physical and chemical properties of materials are strongly correlated with some structural factors, mainly, the structural order–disorder in the lattice.[34] The packing of the constituent clusters of the atoms forming the materials are responsible for the structural order–disorder in the lattice. A specific feature of $Zn_7Sb_2O_{12}$ is the existence of the $[ZnO_4]$ and $[SbO_8]$ clusters as isolated tetrahedron polyhedrons in the crystal lattice, respectively. Therefore, for $Zn_7Sb_2O_{12}$, the material properties can be primarily associated with the tetrahedral $[ZnO_4]$ and heptahedral $[SbO_8]$ cluster constituents. The mismatch of both clusters can induce structural order–disorder effects and will significantly influence the varistor properties of the ZnO. It suggests that distorted $[ZnO_4]$ and $[SbO_8]$ clusters induced the formation of oxygen vacancies being responsible for the varistor properties. Otherwise, it is generally assumed that the electrical properties of varistors are mainly attributed to the charge-transfer transitions within the $[ZnO_4]$ and $[SbO_8]$ complex cluster vacancies according to the following defects reaction:

$$[ZnO_4]^x + [ZnO_3V_O{}^x] \rightarrow [ZnO_4]' + [ZnO_3V_O{}^\bullet] \quad (2)$$

$$[ZnO_4]^x + [ZnO_3V_O{}^\bullet] \rightarrow [ZnO_4]' + [ZnO_3V_O{}^{\bullet\bullet}] \quad (3)$$

$$[SbO_8]^x + [SbO_7V_O{}^x] \rightarrow [SbO_8]' + [SbO_7V_O{}^\bullet] \quad (4)$$

$$[SbO_8]^x + [SbO_7V_O{}^\bullet] \rightarrow [SbO_8]' + [SbO_7V_O{}^{\bullet\bullet}] \quad (5)$$

these defects lead to a high negative electronic density at the grain boundary and a positive charge density in the grain.

$$[ZnO_4]' + [ZnO_3V_O{}^z] + O_2 \rightarrow [ZnO_3V_O{}^z]_{///}O'^{2(ads)} + [ZnO_4]^x \quad (6)$$

$$[SbO_8]' + [SbO_7V_O{}^z] + O_2 \rightarrow [SbO_7V_O{}^z]_{///}O'^{2(ads)} + [SbO_8]^x \quad (7)$$

where $V_O{}^z$ represent a vacancy oxygen $V_O{}^\bullet$ or $V_O{}^{\bullet\bullet}$

$$[ZnO_4]' + [ZnO_3V_O{}^z]_{///}O'_{2(ads)} + [ZnO_3V_O{}^z] \rightarrow [ZnO_4]^x + 2[ZnO_3V_O{}^z]_{///}O'_{(ads)} \quad (8)$$

$$[ZnO_3V_O{}^\bullet]_{///}O'_{(ads)} \rightarrow [ZnO_3V_O{}^{\bullet\bullet}]_{///}O''_{(ads).}$$

For tin oxide the same model can be used emphasizing the higher stability of the cluster complex bonded to oxygen:

$$[SnO_6]' + [SnO_5V_O{}^z] + O_2 \rightarrow [SnO_5V_O{}^z]_{///}O'^{2(ads)} + [SnO_6]^x \quad (9)$$

$$[SnO_6]' + [SnO_5V_O{}^z]_{///}O'^{2(ads)} + [SnO_5V_O{}^z] \rightarrow [SnO_6]^x + 2[SnO_5V_O{}^z]_{///}O'^{(ads)} \quad (10)$$

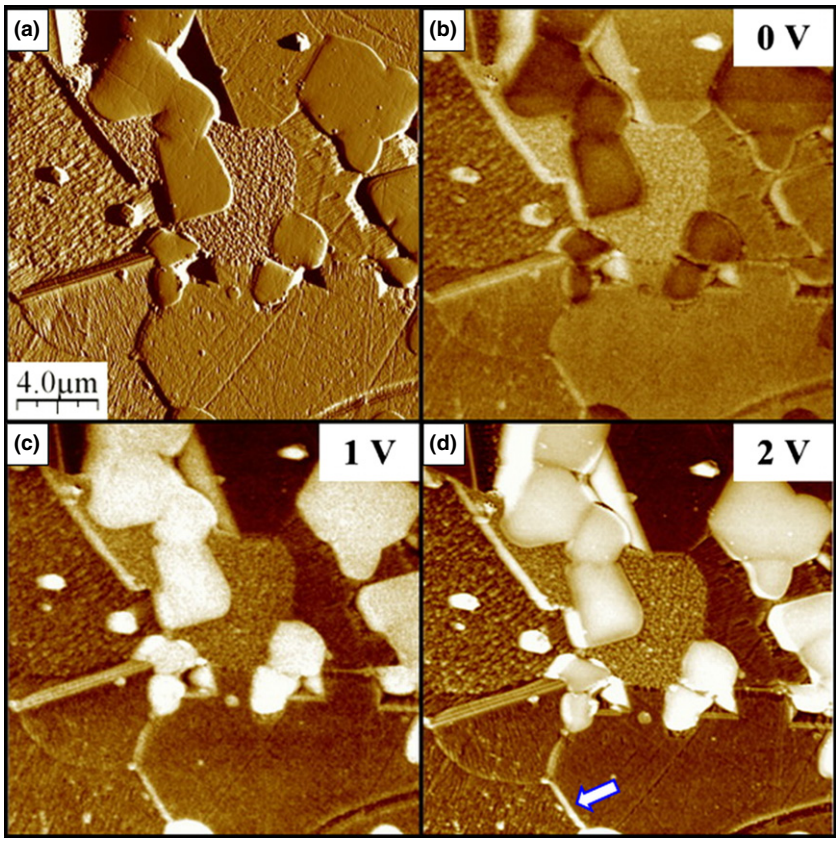

Fig. 5. (a) AFM topographic image of the ZnO-based system after electrical degradation with DC voltage at 110°C. Series of EFM images without applied voltage (b), with applied voltage of 1 V (c), and 2 V (d). In Figure (d), arrows indicate active potential barriers.

Table II. Parameters of the Potential Barrier Using the Model (*C–V*) for the ZnO-Based Varistors After the Degradation Process with DC Voltage

Sample	ϕ_b (eV)	N_d (m^{-3})	N_{ES} (m^{-2})	ω (nm)
ZnO after degradation at 110°C	0.70	5.70×10^{23}	1.95×10^{16}	17.0

Table III. Parameters of the Potential Barrier Using the Model (*C–V*) for Varistors of the SCNCr System After the Degradation Process with DC Voltage

Sample	ϕ_b (eV)	N_d (m^{-3})	N_{ES} (m^{-2})	ω (nm)
SCNCr after degradation at 200°C	1.63	1.55×10^{24}	6.25×10^{16}	20.0

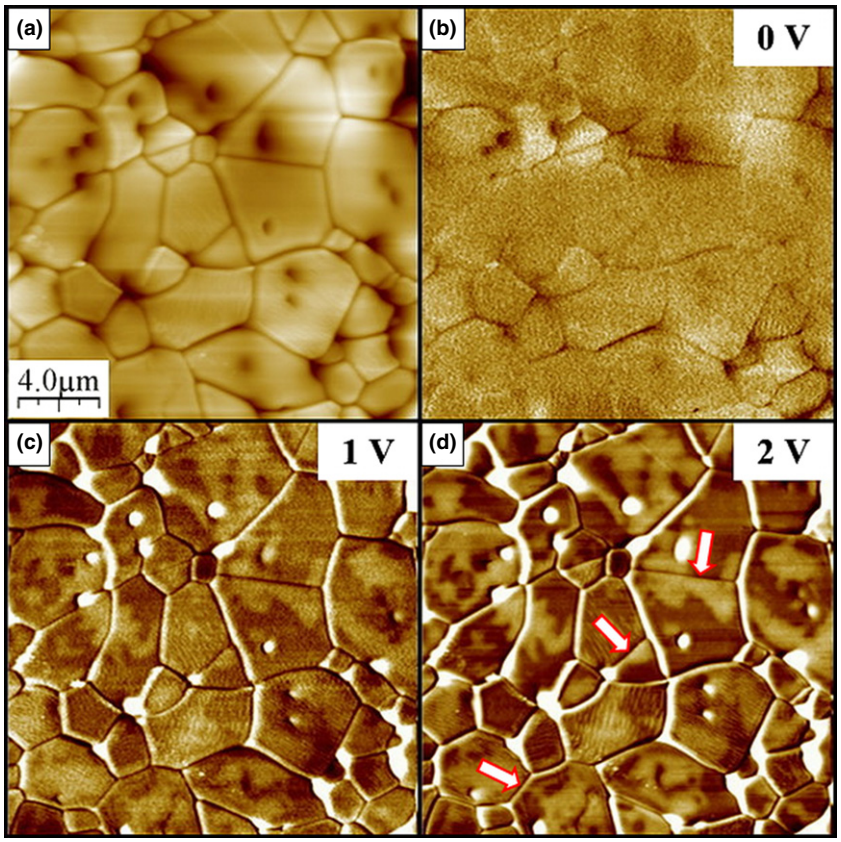

Fig. 6. (a) AFM topographic image of the SCNCr system after electrical degradation with DC voltage at 200°C. Series of EFM images without applied voltage (b), with applied voltage of 1 V (c), and 2 V (d). In Figure (d), arrows indicate inactive potential barriers.

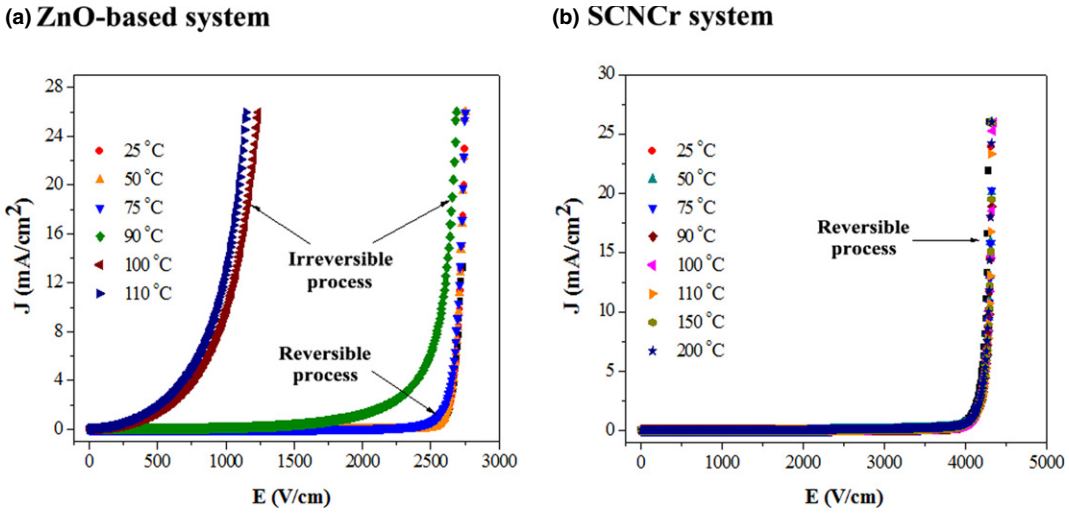

Fig. 7. Evolution of *E–J* curves at different temperatures for DC degradation tests for different varistor systems: (a) ZnO, (b) SnO_2.

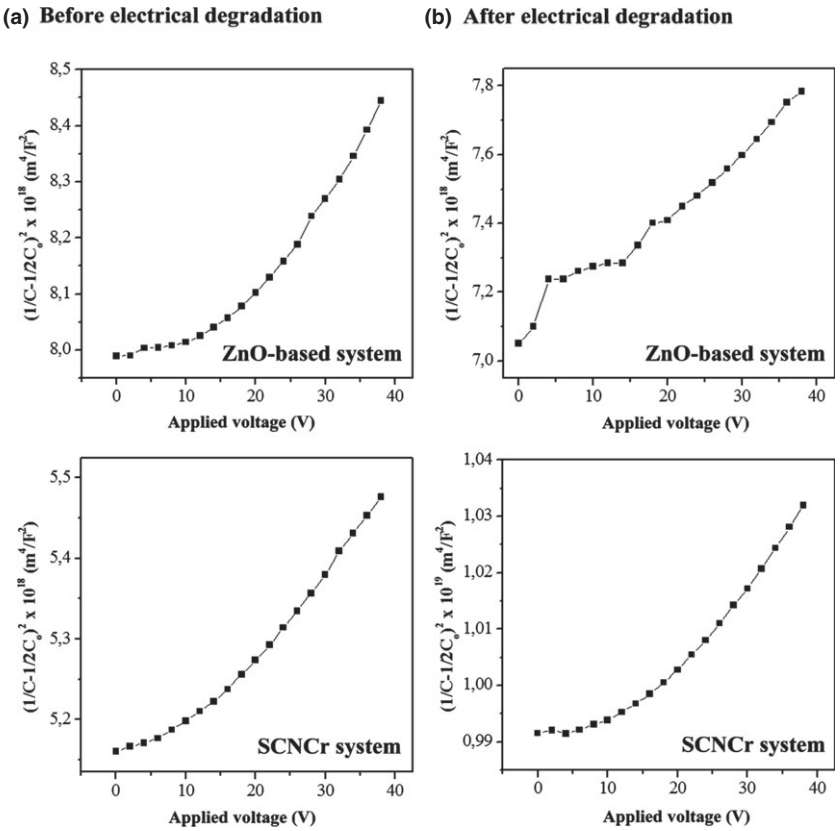

Fig. 8. *C–V* curves for the varistor systems ZnO and SnO_2 (a) before DC degradation and (b) after DC degradation.

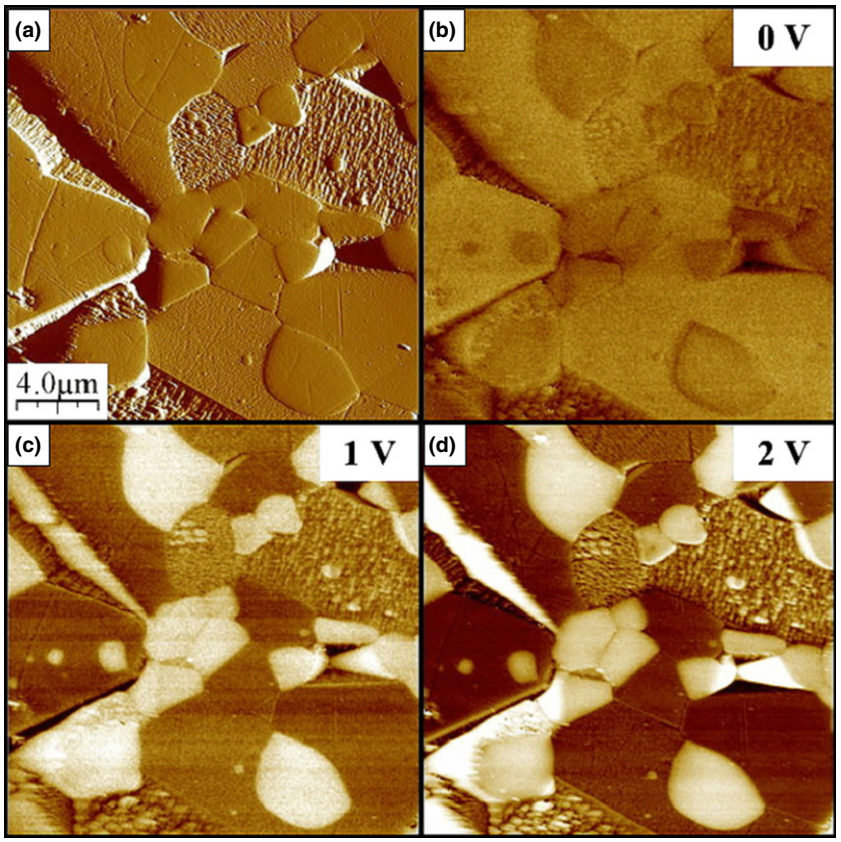

Fig. 9. (a) AFM topographic image of the ZnO-based system after electrical degradation by current pulses. Series of EFM images without applied voltage (b), with applied voltage of 1 V (c), and 2 V (d).

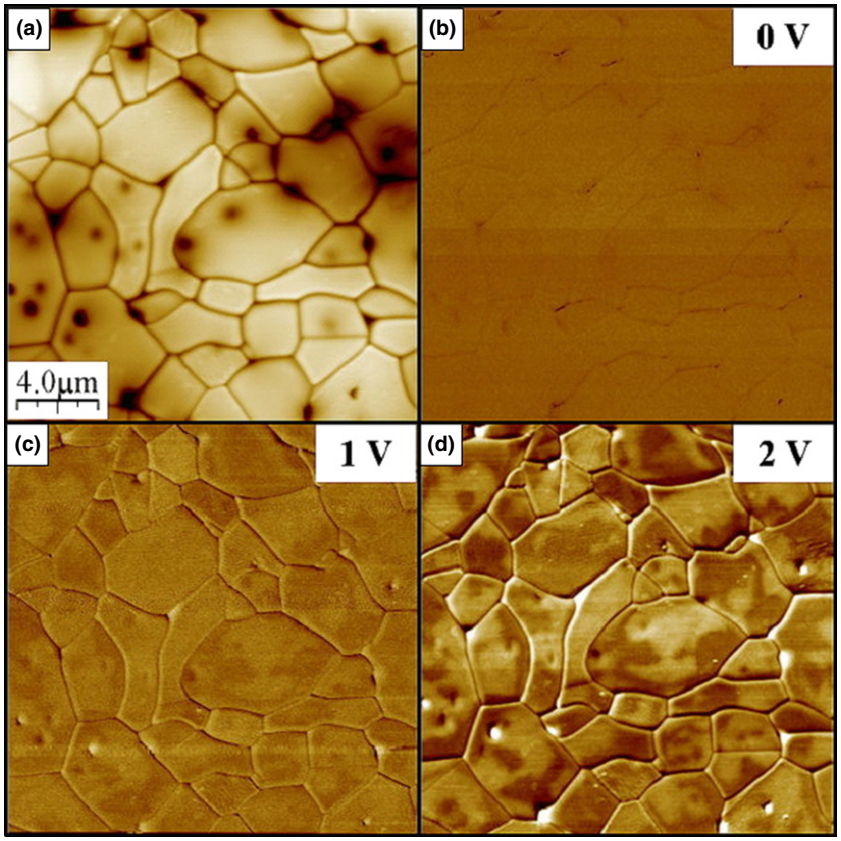

Fig. 10. (a) AFM topographic image of the SCNCr-based system after electrical degradation by current pulses. Series of EFM images without applied voltage (b), with applied voltage of 1 V (c), and 2 V (d).

$$[SnO_5V_O^{\bullet}]_{///}O'_{(ads)} \rightarrow [SnO_5V_O^{\bullet\bullet}]_{///}O''_{(ads)} \quad (11)$$

ZnO–CoMn grains do not present twins. At the interfaces **B** and **C**, the probability of a potential barrier formation is very low, as they belong to the resistive spinel phase. Another possibility of barrier formation would be the interface of the ZnO–Sb phase oriented to the resistive contact with the ZnO–CoMn phase. The morphology of the phases and interfaces in polycrystalline multiphase ZnO-based varistors is complex, which actually explains why there are very few effective barriers, as they are strongly dependent on the orientation of certain grains.

Figure 4 shows the images of AFM and EFM analyses corresponding to the polycrystalline SCNCr system before electrical degradation. Figure 4(a) displays the AFM topographic image of the polished sample thermally etching. Figures 4(b–d) correspond to EFM images under applied voltage range from 0 to 2 V, using a conducting tip. From these images, it becomes evident that the detection of surface charge density is dependent on the applied voltage. In the same way, as was it observed for ZnO-based varistors, applying voltages will change the electrical behavior of the SCNCr system. The dark regions are associated to areas with semiconductive characteristics and the bright regions located primarily at the grain boundaries to charge accumulation regions (effective potential barriers) or insulating regions. An increase in the electric field gradient at the grain boundaries indicates a potential barrier of the Schottky type.

The parameters of the potential barrier were calculated using the model published by Mukae *et al.*[35] and are shown in Table I for both systems before the degradation processes. The percentage of effective barriers[36] in relation to the total number of interfaces calculated from Eq. (1) for images taken under 2 V was 85%. It can be additionally observed from Fig. 4(d) that inside the grains are bright and dark regions. This resistivity anomaly can be explained by chemical compositional fluctuations and nonhomogeneous electrical behavior.

Electrostatic force microscopy analyses revealed that the SCNCr system has a high number of effective barriers (85%) when compared with the ZnO-based system (30%), which was fully expected because of the microstructural homogeneity. This is a positive aspect because homogeneity minimizes percolation paths which generate current concentrations, and consequently thermomechanical failures such as puncturing and/or cracking.[7,10,13] Another advantage is the reduction in material thickness for the same protective voltage level when compared with ZnO-based varistors. With this, it would be possible to fabricate lightning rods of lower weight. However, an appropriated system should be designed to maintain the level of isolation and distances between terminals as recommended by IEEE standards.[37] A disadvantage of the large number of effective barriers in the SCNCr system is the considerable difficulty to manufacture low-voltage varistors.

(2) Sample Properties After Electrical Degradation with DC Voltage

Figure 5 shows the AFM–EFM images of the multiphase polycrystalline ZnO system after electrical degradation with DC voltage at 110°C (thermal runaway temperature). Figure 5(a) shows the AFM topography of the analyzed sample region. The images in Figure 5(b–d) correspond to EFM analyses applying different voltages (0, 1, and 2 V) between the tip and the sample. In this DC voltage degraded system, a significant decrease in the number of effective barriers to 5% is observed. There is also a decrease in the barrier height (as compared with the sample without degradation) as shown in Table II. In addition to influencing the grain boundaries by eliminating much of the effective barriers and reducing the barrier efficiency, the degradation process also affects the electrical response of the grains, a local electrical phenomenon that still has to be studied in detail.

Table IV. Parameters of the Potential Barrier for a Sample of the SCNCr System After Degradation by 8/20 μs Current Pulses

Sample	ϕ_b (eV)	N_d (m^{-3})	N_{ES} (m^{-2})	ω (nm)
SCNCr after degradation	0.52	1.10×10^{24}	2.98×10^{16}	13.5

Analogously, Fig. 6 shows AFM–EFM images of the polycrystalline SCNCr system after the application of DC voltage stress at 200°C. Figure 6(a) is a topographical overview of the sample region obtained by AFM. Figures 6(b–d) correspond with the EFM analysis applying different voltages (0, 1, and 2 V) between the tip and the sample. After imposing the samples to DC voltage stress, no decrease in the number of effective barriers were observed and around 85% of the interfaces were still active indicating the stability of the SCNCr system against DC voltage stress and temperature. This stability was proved by current density versus electric field measurements (*J–E*).

Figure 7 shows the *J–E* behavior for DC voltage and temperature degraded varistors for both, the ZnO system [Fig. 7(a)] and the SnO_2 system [Fig. 7(b)]. The curves provide evidence that the stress did not modify the varistor properties of the SnO_2-based system (even after thermal avalanche at 200°C). For the ZnO-based system, the thermal avalanche occurred at 110°C, and irreversible degradation starts at 90°C, limiting the application of these varistors to temperatures up to 75°C. This observation can be explained by the fact that the SnO_2 system possesses twice the thermal conductivity, thus dissipating more energy and minimizing local heating (Joule effect).

In full agreement with these results, impedance spectroscopy analyses indicate that barrier parameters were not modified as indicated in Table III. These parameters were obtained using the equation by Mukae *et al.*;[35] the *C–V* curves before and after degradation for both systems are given in Fig. 8.

(3) After Electrical Degradation with Current Pulses

AFM–EFM images of the polycrystalline ZnO-based system after degradation through current pulses are given in Fig. 9. By means of a statistical analysis, it was determined that only 1% of the interfaces are effective after the degradation process. As the material did not present any nonohmic behavior after degradation, no potential barrier parameters could be calculated. The image contrast between dark and bright grains in the EFM image of the ZnO system is very low compared with the original sample, indicating more conductive grains with lack of the nonohmic behavior.

An analysis of the SCNCr system using EFM technique (Fig. 10) showed a reduction in the effective interfaces from 85% to 5% of the interfaces. In addition to damaging most of the active interfaces, degradation pulses also affect the electrical response of the grains, and this effect is different for the two materials tested. In the SCNCr system, after degradation the grains were more resistive (lighter colored in Fig. 10) than in the active state. In the ZnO system, after degradation grains are dark colored indicating that they are qualitatively more conductive when compared with the original sample. From these analyses, we can emphasize that EFM is an important tool for monitoring the electrical response of varistors during the degradation processes, corroborating the electrical measurements (Table IV). However, the electrical response of the grains should be studied in more detail.

(4) Proposed Mechanisms for the Electrical Degradation of Potential Barriers

In Fig. 11, schematic diagram before [Figs. 11 (a) and (b)] and after electrical degradation process of the potential barriers with DC voltage [Figs. 11 (c) and (d)] and current pulses [Figs. 11 (e) and (f)] is given. It is noted that solely defects and metastable species are present, which are essentially the same for both systems (oxygen vacancies and adsorbed oxygen atoms). For the ZnO-based system, the presence of interstitial zinc should also be considered. The concentration of defects in the interface is represented by subscript 1 and in the depletion layer by subscript 2. The defect concentration, height (ϕ_B) and width (ω) of potential barriers are repre-

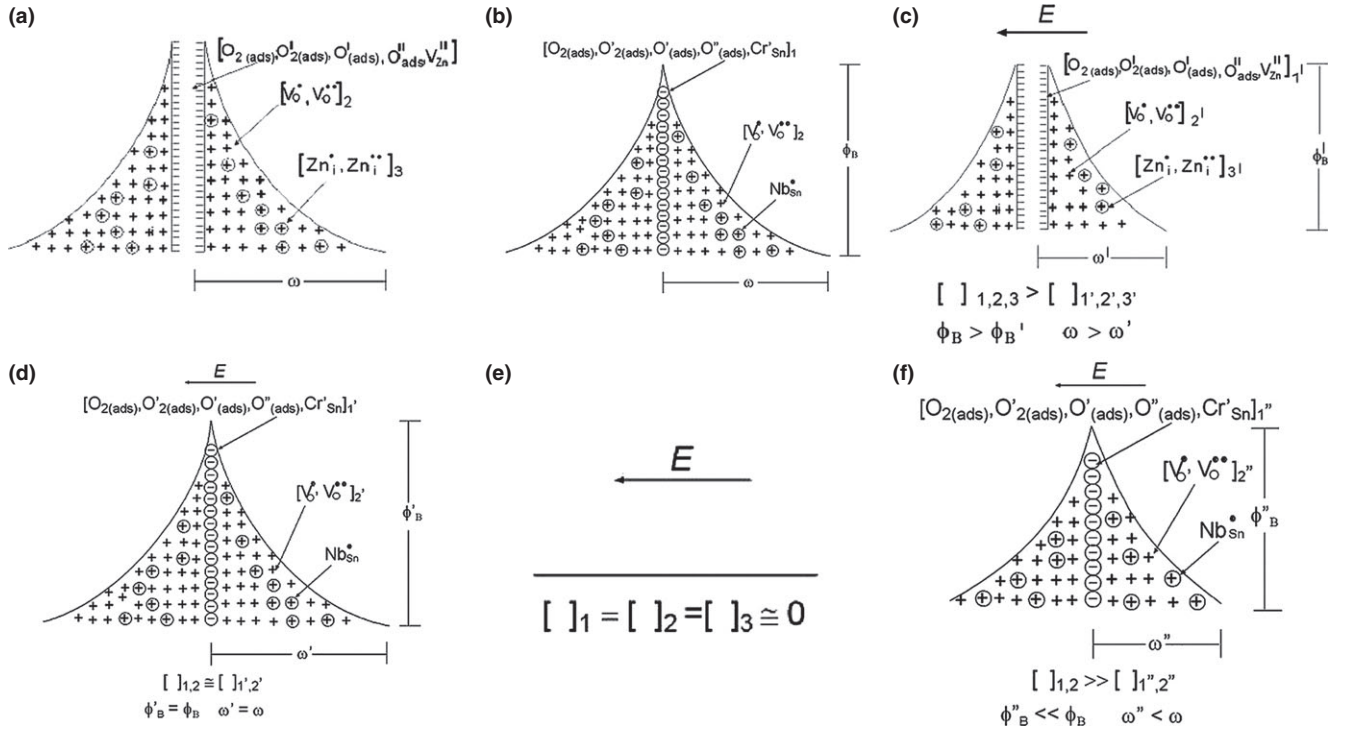

Fig. 11. Schematic diagram for degradation of potential barriers in ZnO-based varistors (a, c, e) and in SCNCr-based varistors (b, d, f), when degradation is due to temperature and DC voltage (c, d) and to 8/20 μs current pulses (e, f).

sented as: (1) Without superscript before degradation, (2) With superscript (′) for DC voltage degradation, and (3) With superscript (″) for pulse degradation.

The SCNCr system does not degrade by applying DC voltage [Fig. 11(d)] ($\varphi'_B = \varphi_B$, $\omega' = \omega$) and the electrical degradation rate with current pulses appears to be lower when comparing with the ZnO-based system, wherein the defect concentration is zero and there are no potential barriers, as the material is conductive. This is due to the fact that this system has a higher number of active barriers and the mobility of metastable defects is lower because the structure is more closed than the hexagonal ZnO wurtzite structure, where all the octahedral sites and half of the tetrahedral sites are unoccupied, and thus, diffusional processes are facilitated.

Figure 11 (c, e, f) depicts the concentrations of metastable defects which decrease during the degradation process. The defect equations best describing the degradation of the barrier in both systems are:

$$[ZnO_3V_O^{\bullet}]_{///}O'_{2(ads)} \rightarrow [ZnO_3V_O^{x}] + O_{2(g)} \quad (12)$$

$$2[ZnO_3V_O^{\bullet}]_{///}O'_{(ads)} \rightarrow 2[ZnO_3V_O^{x}] + O_{2(g)} \quad (13)$$

$$2[ZnO_3V_O^{\bullet\bullet}]_{///}O''_{(ads)} \rightarrow 2[ZnO_3V_O^{x}] + O_{2(g)} \quad (14)$$

$$[SnO_5V_O^{\bullet}]_{///}O'_{2(ads)} \rightarrow [SnO_5V_O^{x}] + O_{2(g)} \quad (15)$$

$$2[SnO_5V_O^{\bullet}]_{///}O'_{(ads)} \rightarrow 2[SnO_5V_O^{x}] + O_{2(g)} \quad (16)$$

$$2[SnO_5V_O^{\bullet\bullet}]_{///}O''_{(ads)} \rightarrow 2[SnO_5V_O^{x}] + O_{2(g)} \quad (17)$$

IV. Conclusions

Due to the microstructural homogeneity of the SCNCr system and the thermodynamics of potential barrier formation, this system has a high number of active interfaces before degradation (85%). The high number of active interfaces in the SCNCr varistor system allows high voltage ratings and small thicknesses. This allows a further reduction in the volume and weight of the up-to-date surge arresters. The ZnO-based system has a heterogeneous microstructure with the presence of different phases and interfaces which explains the low number of active barriers before degradation (30%).

When applying current pulses, for both materials the degradation of the barriers is evident. A degradation by pulses transfers more energy to the material than a degradation by DC voltage, because high currents are involved. This energy is sufficient to activate the diffusion of metastable defects and degrade the potential barriers. However, the SCNCr system was found to be very stable when subjected to degradation with DC voltage and temperature, and the number of active barriers was not changed.

Acknowledgments

The authors gratefully acknowledge the financial support of the Brazilian funding agency FAPESP (Fundação de Amparo à Pesquisa no Estado de São Paulo).

References

[1]D. R. Clarke, "Varistor Ceramics," *J. Am. Ceram. Soc.*, **82**, 485–502 (1999).
[2]M. A. Ramírez, P. R. Bueno, W. C. Ribeiro, D. A. Bonett, J. M. Villa, M. A. Márquez, J. A. Varela, and C. R. Rojo, "The Failure Analyses on ZnO Varistors Used in High Tension Devices," *J. Mater. Sci.*, **40**, 5591–6 (2005).
[3]M. Matsuoka, "Nonohmic Properties of Zinc Oxide Ceramics," *Jpn. J. Appl. Phys.*, **10**, 736–46 (1971).
[4]S. A. Pianaro, P. R. Bueno, E. Longo, and J. A. Varela, "A new SnO_2-Based Varistor System," *J. Mater. Sci. Lett.*, **14**, 692–4 (1995).
[5]M. A. Ramírez, F. R. Marcos, J. F. Fernández, M. Lengauer, P. R. Bueno, E. Longo, and J. A. Varela, "Mechanical Properties and Dimensional Effects of ZnO- and SnO_2 -Based Varistors," *J. Am. Ceram. Soc.*, **91**, 3105–8 (2008).
[6]T. K. Gupta and W. G. Carlson, "A Grain-Boundary Defect Model for Instability/Stability of a ZnO Varistor," *J. Mater. Sci.*, **20**, 3487–500 (1985).
[7]M. A. Ramírez, A. Z. Simões, P. R. Bueno, M. A. Márquez, M. O. Orlandi, and J. A. Varela, "Importance of Oxygen Atmosphere to Recover the ZnO-Based Varistors Properties," *J. Mater. Sci.*, **41**, 6221–7 (2006).
[8]W. I. Lee and R. L. Young, "Defects and Degradation in ZnO Varistor," *Appl. Phys. Lett.*, **69**, 526–8 (1996).
[9]E. R. Leite, J. A. Varela, and E. Longo, "A new Interpretation for the Degradation Phenomenon of ZnO Varistors," *J. Mater. Sci.*, **27**, 5325–9 (1991).
[10]M. A. Ramírez, A. Z. Simões, M. A. Márquez, Y. Maniette, A. A. Cavalheiro, E. Longo, and J. A. Varela, "Characterization of ZnO-Degraded Varistors Used in High-Tension Devices," *Mat. Res. Bull.*, **42**, 1159–68 (2007).
[11]D. Zhou, C. Zhan, and S. Gong, "Degradation Phenomena due to dc Bias in low-Voltage ZnO Varistors," *Mat. Sci. Eng. B*, **99**, 412–5 (2003).
[12]A. Bui, A. Loubiere, and M. Hassanzadeh, "Electrical Characteristics Degradation of ZnO Varistors Subjected to Partial Discharges," *J. Appl. Phys.*, **65**, 4048–50 (1989).
[13]M. A. Ramírez, W. Bassi, P. R. Bueno, E. Longo, and J. A. Varela, "Comparative Degradation of ZnO- and SnO_2-Based Polycrystalline non-Ohmic Devices by Current Pulse Stress," *J. Phys. D: Appl. Phys.*, **41**, 122002, 5pp (2008).
[14]F. A. Modine and R. B. Wheeler, "Pulse Response Characteristics of ZnO Varistors," *J. Appl. Phys.*, **67**, 6560–6 (1990).
[15]T. K. Gupta and W. G. Carlson, "Barrier Voltage and its Effect on Stability of ZnO Varistor," *J. Appl. Phys.*, **53**, 7401–9 (1982).
[16]M. A. Ramírez, M. Cilense, P. R. Bueno, E. Longo, and J. A. Varela, "Comparison of non-Ohmic Accelerated Ageing of the ZnO- and SnO_2-Based Voltage Dependent Resistors," *J. Phys. D: Appl. Phys.*, **42**, 015503, 4pp (2009).
[17]M. Tao, A. Bui, O. Dorlanne, and A. Loubiere, "Different Single Grain Junctions Within a ZnO Varistor," *J. Appl. Phys.*, **61**, 1562–7 (1987).
[18]Z. C. Cao, R. J. Wu, and R. S. Song, "Ineffective Grain-Boundaries and Breakdown Threshold of Zinc-Oxide Varistors," *Mater. Sci. Eng., B*, **22**, 261–6 (1994).
[19]H. Wang, W. Li, and J. F. Cordaro, "Single Junctions in ZnO Varistors Studied by Current-Voltage Characteristics and Deep-Level Transient Spectroscopy," *Jpn. J. Appl. Phys.*, **34**, 1765–71 (1995).
[20]H. Wang, W. A. Schulze, and J. F. Cordaro, "Averaging Effect on Current-Voltage Characteristics of ZnO Varistors," *Jpn. J. Appl. Phys.*, **34**, 2352–8 (1995).
[21]Q. Wen and D. R. Clarke, "Grain Boundaries and Interfacial Phenomena in Electronic Ceramics"; pp. 217–30 In: *Ceramic Transactions*, Vol. **41**, Edited by L. M. Levinson and S. I. Hirno. American Ceramics Society, Westerville, OH, 1994.
[22]S. V. Kalinin, R. Shao, and D. A. Bonnell, "Local Phenomena in Oxides by Advanced Scanning Probe Microscopy," *J. Am. Ceram. Soc.*, **88**, 1077–98 (2005).
[23]P. Girard, "Electrostatic Force Microscopy: Principles and Some Applications to Semiconductors," *Nanotechnology*, **12**, 485–90 (2001).
[24]A. Doukkali, S. Ledain, C. Guasch, and J. Bonnet, "Surface Potential Mapping of Biased pn Junction With Kelvin Probe Force Microscopy: Application to Cross-Section Devices," *Appl. Surf. Sci.*, **235**, 507–12 (2004).
[25]M. A. De la Rubia, M. Peiteado, J. F. Fernández, and A. C. Caballero, "Compact Shape as a Relevant Parameter for Sintering ZnO-Bi_2O_3 Based Varistors," *J. Eur. Ceram. Soc.*, **24**, 1209–12 (2004).
[26]M. A. Ramírez, J. F. Fernández, M. De la Rubia, J. De Frutos, P. R. Bueno, E. Longo, and J. A. Varela, "The Influence of Area/Volume Ratio on Microstructure and non-Ohmic Properties of SnO_2-Based Varistor Ceramic Blocks," *J. Mater. Sci.: Mater. Electron.*, **20**, 49–54 (2009).
[27]M. A. Ramirez, W. Bassi, R. Parra, P. R. Bueno, E. Longo, and J. A. Varela, "Comparative Electrical Behavior at low and High Current of SnO_2 and ZnO-Based Varistors," *J. Am. Ceram. Soc.*, **91**, 2402–4 (2008).
[28]J. S. Vasconcelos, N. S. L. S. Vasconcelos, M. O. Orlandi, P. R. Bueno, J. A. Varela, E. Longo, C. M. Barrado, and E. R. Leite, "Electrostatic Force Microscopy as a Tool to Estimate the Number of Active Potential Barriers in Dense non-Ohmic Polycrystalline SnO_2 Devices," *Appl. Phys. Lett.*, **89**, 152102 (2006).
[29]P. R. Bueno, M. A. Santos, M. A. Ramirez, R. Tararam, E. Longo, and J. A. Varela, "Relationship Between Grain-Boundary Capacitance and Bulk Shallow Donors in SnO_2 Polycrystalline Semiconductor," *Phys. Status Solidi A*, **205**, 1694–8 (2008).
[30]A. Recnik, N. Daneu, T. Walther, and W. Mader, "Structure and Chemistry of Basal-Plane Inversion Boundaries in Antimony Oxide-Doped Zinc Oxide," *J. Am. Ceram. Soc.*, **84**, 2657–68 (2001).
[31]U. Schwing and B. Hoffmann, "Model Experiments Describing the Microcontact of ZnO Varistors," *J. Appl. Phys.*, **57**, 5372–9 (1985).
[32]E. Olsson and G. L. Dunlop, "Characterization of Individual Interfacial Barriers in a ZnO Varistor Material," *J. Appl. Phys.*, **66**, 3666–75 (1989).
[33]M. S. Castro, M. P. Suarez, and C. M. Aldao, "STM and STS Analysis of ZnO Varistors," *Bol. Soc. Esp. Ceram.*, **41**, 143–6 (2002).
[34]F. Stucki and F. Greuter, "Key Role of Oxygen at Zinc-Oxide Varistor Grain-Boundaries," *Appl. Phys. Lett.*, **57**, 446–8 (1990).
[35]K. Mukae, K. Tsuda, and I. Nagasawa, "Capacitance-vs-Voltage Characteristics of ZnO Varistors," *J. Appl. Phys.*, **50**, 4475–6 (1979).
[36]V. P. B. Marques, M. Cilense, P. R. Bueno, M. O. Orlandi, J. A. Varela, and E. Longo, "Qualitative Evaluation of Active Potential Barriers in SnO_2-Based Polycrystalline Devices by Electrostatic Force Microscopy," *Appl. Phys. A Mater. Sci. Process.*, **87**, 793–6 (2007).
[37]Surge Arresters – Part 5: Selection and Application Recommendations. IEC 60099-5, 1st edition, 1996–2002. □